AGU PUBLICATIONS

JGR

Journal of Geophysical Research: Solid Earth

RESEARCH ARTICLE
10.1002/2016JB013244

Key Points:
- The Moho inside of MCR is underplated by magmatic rocks
- Shallowing of both sedimentary and extruded igneous layers is observed
- The Moho outside of the MCR is sharp and flat

Supporting Information:
- Supporting Information S1
- Figure S1
- Figure S2
- Figure S3
- Figure S4
- Figure S5
- Figure S6
- Figure S7

Correspondence to:
H. Zhang,
hzhang@earth.northwestern.edu

Citation:
Zhang, H., et al. (2016), Distinct crustal structure of the North American Midcontinent Rift from *P* wave receiver functions, *J. Geophys. Res. Solid Earth*, *121*, doi:10.1002/2016JB013244.

Received 4 JUN 2016
Accepted 30 OCT 2016
Accepted article online 7 NOV 2016

Distinct crustal structure of the North American Midcontinent Rift from *P* wave receiver functions

Hao Zhang[1], Suzan van der Lee[1], Emily Wolin[1], Trevor A. Bollmann[1], Justin Revenaugh[2], Douglas A. Wiens[3], Andrew W. Frederiksen[4], Fiona A. Darbyshire[5], Ghassan I. Aleqabi[3], Michael E. Wysession[3], Seth Stein[1], and Donna M. Jurdy[1]

[1]Department of Earth and Planetary Sciences, Northwestern University, Evanston, Illinois, USA, [2]Department of Earth Sciences, University of Minnesota, Minneapolis, Minnesota, USA, [3]Department of Earth and Planetary Sciences, Washington University in St Louis, St. Louis, Missouri, United States, [4]Department of Geological Sciences, University of Manitoba, Winnipeg, Manitoba, Canada, [5]Centre de recherche GEOTOP, University of Quebec at Montreal, Montreal, Quebec, Canada

Abstract Eighty-two broadband seismic stations of the Superior Province Rifting Earthscope Experiment (SPREE) collected 2.5 years of continuous seismic data in the area of the high gravity anomaly associated with the Midcontinent Rift (MCR). Over 100 high-quality teleseismic earthquakes were used for crustal *P* wave receiver function analysis. Our analysis reveals that the base of the sedimentary layer is shallow outside the MCR, thickens near the flanks where gravity anomalies are low, and shallows again in the MCR's center where the gravity anomalies peak. This pattern is similar to that found from local geophysical studies and is consistent with reverse faulting having accompanied the cessation of rifting at 1.1 Ga. Intermittent intracrustal boundaries imaged by our analysis might represent the bottom of the MCR's mostly buried dense volcanic layers. Outside the MCR, the Moho is strong, sharp, and relatively flat, both beneath the Archean Superior Province and the Proterozoic terranes to its south. Inside the MCR, two weaker candidate Mohos are found at depths up to 25 km apart in the rift's center. The intermediate layer between these discontinuities tapers toward the edges of the MCR. The presence of this transitional layer is remarkably consistent along the strike of the MCR, including beneath its jog in southern Minnesota, near the Belle Plaine Fault. We interpret these results as evidence for extensive underplating as a defining characteristic of the rift, which remains continuous along the Minnesota jog, where due to its orientation, it is minimally affected by the reverse faulting that characterizes the NNE striking parts of the rift.

1. Introduction

The midcontinent geophysical anomaly (MGA) marks a 1.1 Ga old, 30 Myr long failed attempt to rift apart Laurentia, North America's Precambrian core [*Van Schmus et al.*, 1982; *Hinze et al.*, 1997]. The structure and composition of the crust of this Midcontinent Rift (MCR) was substantially changed by thermal and magmatic events, as well as by subsidence, faulting, sedimentation, and later compression, which caused intense gravity and magnetic anomalies along this structure [*Keller et al.*, 1980; *Hinze et al.*, 2005; *King and Zietz*, 1971]. The most prominent portion of the MGA lies beneath Lake Superior, follows the Minnesota-Wisconsin border southward, and then curves west in Iowa. The mechanisms of the formation and evolution of the MCR are still under debate. The thermal perturbation of a mantle plume or hotspot has been invoked as the active origin of the rifting [e.g., *Green*, 1982; *Allen et al.*, 1992; *Vervoort et al.*, 2007]. Alternatively, far-field stresses related to the Grenville orogeny have been invoked as a cause of passive rifting [e.g., *McWilliams and Dunlop*, 1978; *Gordon and Hempton*, 1986]. *Miller and Nicholson* [2013] provide a concise overview of the evidence for and against a plume source for the MCR's volcanic rocks.

Whereas some aspects, in particular the near-surface crustal structure of the MCR, have been studied using gravity and magnetic anomalies [e.g., *Thiel*, 1956; *King and Zietz*, 1971], more detailed views, especially at depth necessitate seismological investigations. The Great Lakes International Multidisciplinary Program on Crustal Evolution (GLIMPCE) was an active source seismic reflection and refraction study carried out in the 1980s [*Cannon et al.*, 1989; *Tréhu et al.*, 1991]. Several GLIMPCE lines were shot in Lake Superior, which is underlain by the MCR. Of GLIMPCE lines, GLIMPCE line A (Figure 1) is the longest and thereby the only line in

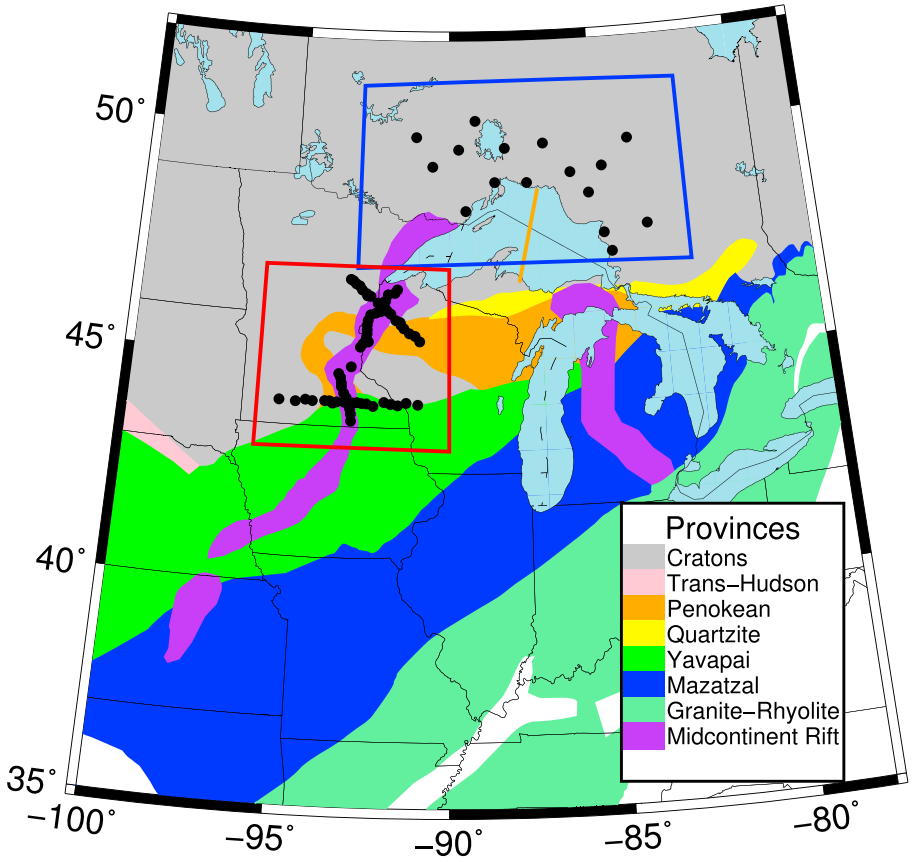

Figure 1. Precambrian tectonic provinces around the North American MCR [after *Whitmeyer and Karlstrom*, 2007]. Black dots: SPREE project stations. The blue and red boxes indicate the MCR and Canadian craton subarrays, shown in Figure 2. The GLIMPCE-A seismic profile is shown as a pink line.

the area that detected seismic energy reflected from near-Moho depths. The depth of the deepest imaged interface changes along the line from 40 to 55 km beneath the center of the MCR, while a secondary deep interface rises beneath the rift to as shallow as 25 km [e.g., *Cannon et al.*, 1989; *Tréhu et al.*, 1991; *Thomas and Teskey*, 1994; *Miller and Nicholson*, 2013]. Tens-of-kilometers thick stacks of volcanic rocks were inferred to lie beneath sediments [*Green et al.*, 1989; *Ojakangas et al.*, 2001]. These stacks are thickest beneath the central gravity high of the MGA and thin away from the rift over several to tens of kilometers laterally. Also, reversed faulting has been inferred to overprint the normal faulting within the rift's flanks [*Behrendt et al.*, 1988]. *French et al.* [2009] studied receiver functions from Florida-to-Edmonton (FLED) broadband seismic stations that crossed the MCR in Iowa. Beneath the MCR, they found stronger depth variances in the presumed Moho than anywhere else along the FLED line. The FLED RFs, shown by *Moidaki et al.* [2013], show a clear Moho for station FA18 outside of the MGA, but considerable complexities for stations within the rift, documenting weaker interfaces at depths up to 15 km apart with a cross-rift distance of several dozen kilometers. The shear-wave velocities of the lithosphere around the western arm of the MCR were estimated by *Shen et al.* [2013] from ambient seismic noise group and phase velocities from more than 120 Earthscope/US Transportable Array (TA) broadband seismic stations. While their phase and group velocity data are clearly slow along the MCR, it is unclear which fractions of this slowness should be ascribed to a thick crust, relatively low crustal *S* velocities, or simply to the relatively high density of the voluminous, shallow volcanic rocks. We now report on crustal structure and interface depths beneath three denser lines of broadband seismic stations that span about 400 km along and across the MCR and beneath additional reference stations in central Ontario.

The Superior Province Rifting Earthscope Experiment (SPREE) aimed to resolve the high-resolution structure of the crust and upper mantle of the main branch of the MCR near the Lake Superior and the Minnesota-Wisconsin border. Here we focus on the crust-mantle transition beneath the MCR as well as intracrustal

layers such as sedimentary strata and midcrustal discontinuities using *P* wave receiver functions (RFs) at the 82 SPREE stations.

2. Data and Methodology

2.1. SPREE

SPREE comprises four broadband station groups (SC, SN, SM, and SS), 82 stations in total, distributed around the MCR as shown in Figure 2. Station line SN crosses the MCR north of Minneapolis-St. Paul in a roughly NW-SE direction, while the roughly E-W trending station line SS crosses the MCR in southern Minnesota. Station line SM consists of two segments along the MCR, which intersect line SN in the north and line SS in the south, respectively. Additionally, the subgroup SC, a two-dimensional array, is located in the Superior Province of the Canadian Shield north of Lake Superior (Figure 2a). The average station spacings of the SN, SM, and SS profiles are ~12 km, much shorter than the ~70 km of the subgroup SC and USArray, allowing for higher resolving power at the scale of the MCR's width.

The SPREE stations were deployed for 2.5 years between April 2011 and October 2013 [*Wolin et al.*, 2015]. We visually inspected three-component SPREE seismograms of teleseismic earthquakes with magnitudes over M_w 5.5 that occurred during this period from 30° to 90° from the array's center (Figure 3a). A total of 119 earthquakes remained after a visual check to exclude earthquakes having low-quality *P* wave trains. Figures 3a and 3b show the distribution of these earthquakes geographically and with back-azimuth. The back-azimuthal distribution points to two distinct and active subduction zones, the northwest Pacific (300° – 330°) and western South America (150° – 180°). All earthquakes retained have magnitudes greater than M_w 5.8, with the most frequent magnitude being around M_w 6.1. Because of varying water cycles and soil conditions from station to station and season to season [*Wolin et al.*, 2015], some earthquakes are recorded with far more seismic noise and *P* arrival-generated soft-sediment reverberations at some stations than others. Nevertheless, all stations retain at least 10 high-quality seismograms and the average number of seismograms retained per station is ~30.

2.2. Time Domain Receiver Functions

Receiver function analysis is a commonly used method to investigate discontinuities in the crust and mantle [e.g., *Vinnik*, 1977; *Langston*, 1979; *Ligorría and Ammon*, 1999]. Receiver functions (RF) highlight converted *S* arrivals that are generated by the primary *P* waves impinging on a layer interface. The RFs are calculated by deconvolving the vertical-component seismogram, which is dominated by the direct *P* arrival, from the radial-component seismogram, which contains these converted *S* arrivals. Traditionally, the deconvolution was more efficiently carried out in the frequency domain than in the time domain. However, iterative time domain deconvolution leads to more stable results, in particular for noisy stations [*Ligorría and Ammon*, 1999].

To obtain the SPREE RF, we first rotated the horizontal *E* and *N* component seismograms to the radial and transverse components for each earthquake and station. An iterative time-domain deconvolution was applied to the 100 s long rotated three-component seismograms (10 s before the first *P* arrivals) with a maximum of 800 iterations. We used a low-pass Gaussian filter factor a of 2.5, which is equivalent to weighting and averaging the RF values with a moving ~1 s wide Gaussian pulse [*Ligorría and Ammon*, 1999]. Next, visual inspection and further culling of RFs with a cross-correlation coefficient below 0.6 with the stacked RF for each SPREE station provided 2624 RFs for structural analysis. Figures 3c – 3e show RF stacks for three SPREE stations.

RFs recorded at stations inside the rift's gravity high show more complexity than those recorded at stations outside of the gravity high (Figures 3c – 3e). For example, for station SS83 outside of the gravity high, RFs consistently show a *P*-to-*S* converted wave (P_ms) at ~5 s for both groups of events with opposing azimuthal ranges. However, for station SN55 inside the gravity high, for example, RFs from the northern and northwestern Pacific subduction zones (Aleutians, Kamchatka, Kuril, Japan) show a clear P_ms peak at ~4.2 s, while RFs from South American events show more ambiguous and possibly multiple P_ms arrivals around ~6.6 s. Additionally, *P*-to-*S* waves converted at a midcrustal discontinuity (P_ds) are observed at several SPREE stations, both inside and outside the gravity high. Figure 3c shows RFs for station SN47 as an example of where a P_ds is observed. RFs for other stations are provided in Figures S1 – S5 in the supporting information.

The strong bimodal azimuthal dependence of both the timing and strength of *P*-to-*S* converted phases suggests that there is more than one interface around the depth where we typically find the Moho outside the gravity high. The high-energy transverse components of RFs inside the gravity high indicate that some of these interfaces are at least dipping, if not anisotropic or more complex.

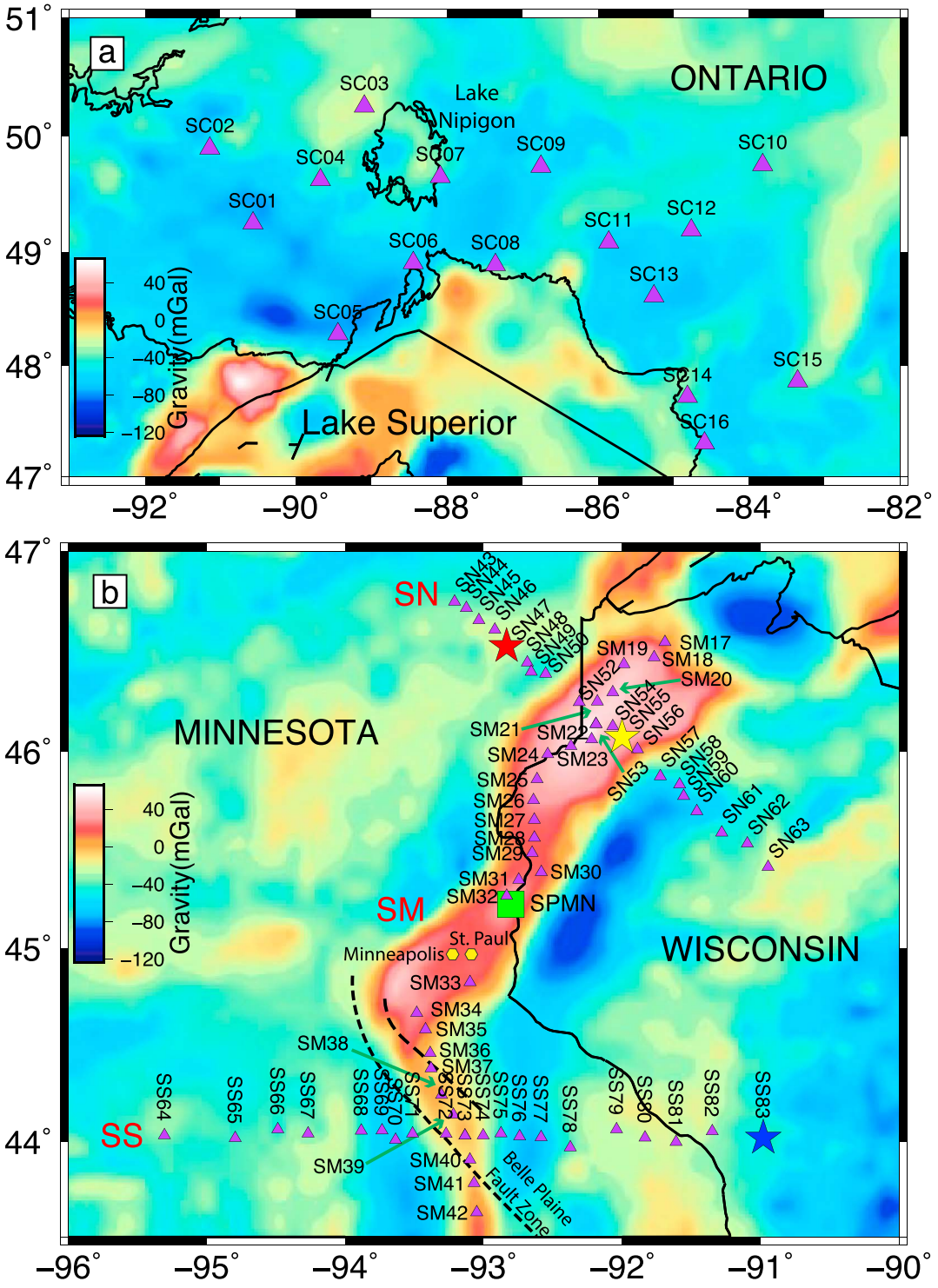

Figure 2. Stations (purple triangles) and Bouguer gravity anomaly [*Keller et al.*, 1980; *Hinze et al.*, 2005] around the (a) Canadian craton and (b) MCR subregions. The MCR network is divided into three linear profiles, SS, SM, and SN. Stations SN47 (red star), SN55 (yellow star), and SS83 (blue star) are treated in detail in the text. The Belle Plaine Fault Zone (dashed lines) from *Sims* [1987] coincides roughly with the gravity high's jog as well as the southern part of the SM line (SM34–SM42) and obliquely intercepts with the SS line (SS64–SS83). Permanent station SPMN is shown by a green square.

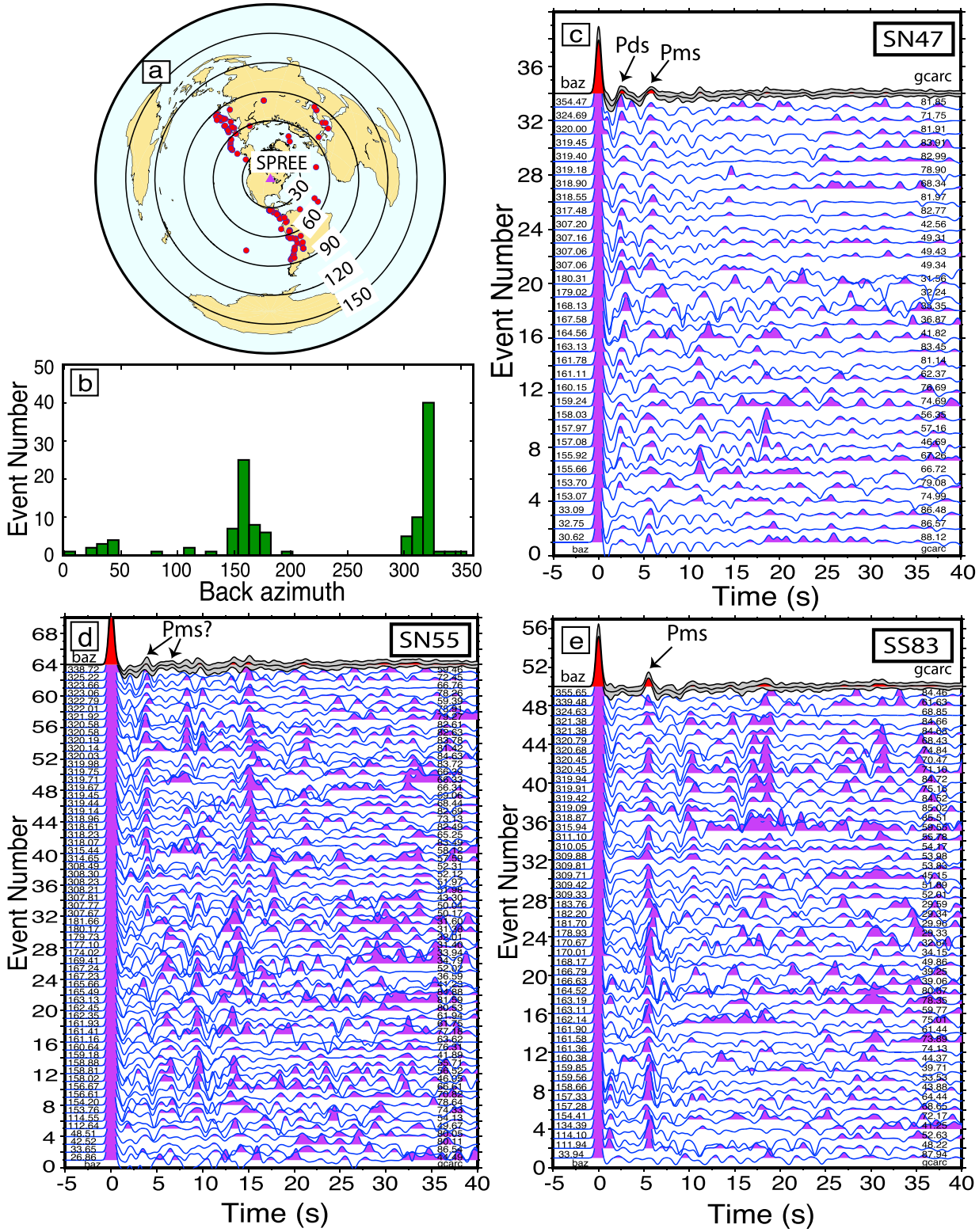

Figure 3. (a) Distribution of 119 earthquakes (red circles) recorded at 82 SPREE stations. The center of the SPREE stations is at (45.268°N, 92.834°W). (b) Event distribution as a function of back-azimuth. Events mainly originate from South America and Northeast Asia. *P* wave receiver functions at three typical stations: (c) SN47, (d) SN55, and (e) station SS83. Top trace with red infill is the stacked waveform. The gray zone indicates standard error range. Significantly positive and negative peaks are colored red and blue, respectively. The numbers labeled on the left indicate back azimuths of the events, and the numbers labeled on the right indicate epicentral distances. Inside of the MCR at station SN55, *P*-to-*S* waves converted at multiple discontinuities are labeled with P_ms at ~4 s and/or at ~6.6 s. The P_ds phase at SN47 implies a midcrustal discontinuity.

2.3. H-κ Stacking

The H-κ stacking method (HKS) is a grid search technique that finds the optimal values for the crustal thickness H and κ, where $\kappa = \alpha/\beta$, and α and β are the P and S velocities, respectively, found by maximizing the sum of the weighted sums of the individual RF values at three predicted arrival times that correspond to the P_ms and the two sets of crustal multiples (PpP_ms and $PsP_ms + PpS_ms$) [*Zhu and Kanamori*, 2000]. Although minimal, differences in phase move-out with epicentral distance are thus taken into account. An important assumption for predicting the arrival times of these phases is that the crustal interfaces are horizontal and that the crustal layers are laterally homogeneous and isotropic. Given a pair of H (crustal thickness) and κ values, the summed amplitude is expressed as

$$S(H,\kappa) = \sum_{i=1}^{N} \left[w_1 r_i \left(t_{P_ms} \right) + w_2 r_i \left(t_{PpP_ms} \right) - w_3 r_i \left(t_{PsP_ms} \right) \right], \quad (1)$$

where w_1, w_2, and w_3 are the weights of three phases P_ms, PpP_ms, and PpS_ms+PsP_ms, respectively, t_{P_ms}, t_{PpP_ms}, and t_{PsP_ms} are the predicted arrival times of the three phases, N is the number of events, and $r_i(t)$ is the RF derived from the ith event.

The value of $S(H,\kappa)$ is most sensitive to H and κ and least sensitive to the value of the P wave velocity α [*Zhu and Kanamori*, 2000]. We assigned α of the crust to be 6.456 km/s (average P velocity of the North American crust) and α of the mantle to be 8.033 km/s (P velocity of the uppermost mantle) [*Chulick and Mooney*, 2002]. The κ was searched from 1.55 to 2.05 while the crustal thickness H was scanned from 30 km to 70 km. After trying a series of values, we set the weights w_1, w_2, and w_3 as 0.4, 0.3, and 0.3 on a basis of signal-to-noise ratios of the three phases and imaging quality.

The values of $S(H,\kappa)$ are shown in Figures 4a and 4b for stations SN55 and SS83. Station SS83 shows a clear global maximum between 44 and 48 km for crustal thickness H and a κ between 1.67 and 1.73. The curved nature of the band of local maxima that extends to the lower left and upper right from the global maximum illustrates the strong trade-off between H and κ in explaining a P-to-S conversion from a single interface. The values of $S(H,\kappa)$ for station SN55 show multiple maxima that do not all lie in each other's extensions along trade-off curves, indicating the presence of multiple interfaces at different depths or possibly intracrustal multiples [*Zhu and Kanamori*, 2000]. The global maximum is found for a discontinuity at a depth of 39 ± 2 km with a relatively low κ of 1.58. A local maximum could indicate a discontinuity at 49 ± 4 km depth with a relatively high κ of 1.80. The former is consistent with the labeled Moho peak in the stack of only data from events in Northeast Asia (Figure 4e). The latter is consistent with a broadened Moho peak in the stack of only data from events in South America (Figure 4f). If we assume that the strongest velocity contrast at the global maximum represents the Moho, it would mean that the Moho beneath the MGA is shallower than the Moho outside of the MGA. However, the mantle might not begin until below the deeper interface associated with the local maximum in $S(H,\kappa)$.

The uncertainties in the crustal thickness and κ were estimated from the standard deviation of the summed amplitude $S(H,\kappa)$ [*Zhu and Kanamori*, 2000]. The horizontal uncertainty δh is estimated as the standard deviation of the horizontal distribution of conversion points at the Moho.

2.4. Waveform Fitting for RFs

A one-dimensional space was grid searched for the optimal thickness H of the crust, between 30 and 65 km, that produced the best waveform fit of the RFs' stack (Figures 4c and 4d). We introduce a new way of visualizing the uncertainty in the values of the RF stack; we plot the error as a gray area around a value and only color fill the RF values that exceed the error value. The P velocity was fixed to 6.456 km/s, and κ was set to either those derived from the H-κ analysis within a reasonable range of 1.65–1.9 or the default value of 1.73 for stations with κ out of the range. For stations like station SN47 having RFs with P-to-S converted at the midcrustal discontinuity, a two-layered crustal model based on the uppermost portion of the NA04 tomographic model of *Van der Lee and Frederiksen* [2005] was used to calculate the initial synthetic RF.

We also use the waveform fitting method [*Van der Meijde et al.*, 2003] to determine the thickness of the sedimentary cover. For each station, the RFs are slant stacked using a reference ray parameter of 0.06 s/km. The sedimentary layer, if present, is constrained by finding the optimal values for thickness and κ of the sedimentary layer that produce the synthetic RF that best fits the RF stack up to several seconds after the P arrival (Figures 4c and 4d). This waveform fitting method is sensitive to sedimentary layers because they

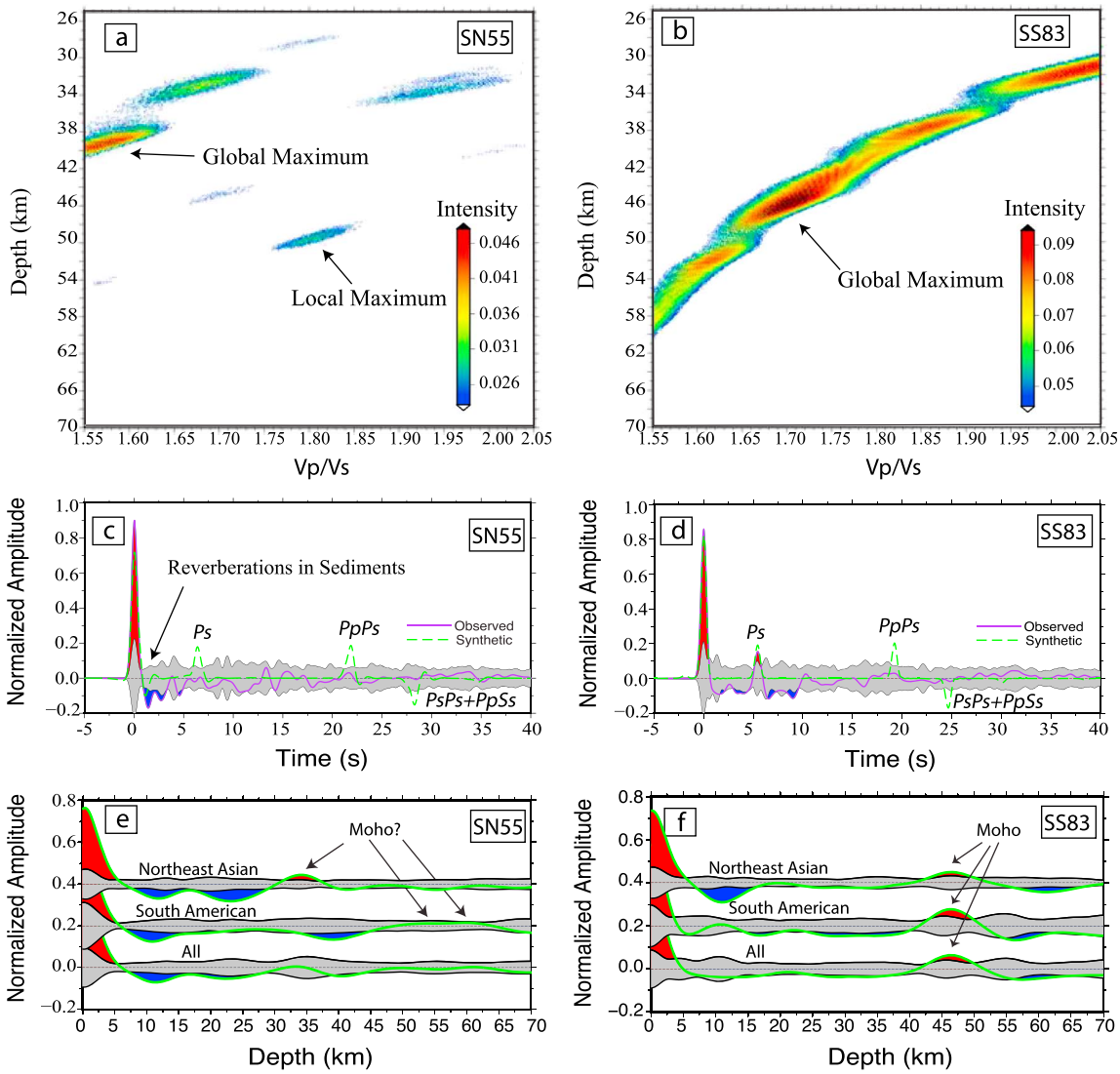

Figure 4. *H*-κ stacking (HKS) results for stations (a) SN55 and (b) SS83 and synthetic RF stacks for stations (c) SN55 and (d) SS83. Top trace with red infill is the stacked waveform. The gray zone indicates standard error range. Significantly positive and negative peaks are colored red and blue, respectively. Also shown are stacked RFs in the depth domain for stations (e) SN55 and (f) SS83. For SN55, the stacked RFs are derived from Northeast Asian, South American, and all events, respectively. Migration is based on the *S* velocity from model NA04, not taking varying of values into account. The gray zones indicate the standard error domain.

cause small apparent shifts in the RF's *P* arrival as well as strong multiples immediately following the RF's *P* arrival [*Van der Meijde et al.*, 2003]. Rather than fixing the *P* velocity as in the *H*-κ method, we grid searched a three-dimensional parameter space for the best *S* velocity between 0.5 km/s and 3.5 km/s, the best κ between 1.55 and 2.05 and the best thickness within a range of 0.0–5.0 km. Density is given by the relationship with *P* wave velocity $\rho(V_p) = 0.77 + 0.32 \times V_p$ [*Berteussen*, 1977].

Mantle values are fixed to the average mantle of the midcontinent of North America [*Chulick and Mooney*, 2002; *Van der Lee and Frederiksen*, 2005]. The 45 s long synthetic RFs, including 5 s of signal before the first *P* arrival, are computed with the reflectivity method of *Kennett* [1979]. Thus, these synthetic RFs contain waveforms of the main phases P_ms, PpP_ms, and $PpS_ms + PsP_ms$ as well as conversions and multiples from within the sedimentary strata. Additionally, for some stations along the profile SN, such as SN47, the grid search results suggest the presence of an extra midcrustal discontinuity, whose depth is estimated based on the average 1-D velocity model of NA04 [*Van der Lee and Frederiksen*, 2005].

The uncertainties in sedimentary thickness H_s and thicknesses H_d of the Moho or intracrustal discontinuities are estimated in different ways. For the sedimentary layer, the uncertainty in the stack is used via waveform

fitting of the stack and the stack plus one standard error to estimate the uncertainty in H_s. For the Moho or the intracrustal discontinuities, the half width δt of the corresponding $P_d s$ peak was taken to estimate the uncertainty of H_d :

$$\delta H = \delta t \times H_d / t_{P_d s},$$

where $t_{P_d s}$ is the arrival time of the *P*-to-*S* converted wave at the discontinuity *d* relative to the direct *P* wave. This estimate includes the consequences of filtering.

For the Moho or intracrustal discontinuities, the horizontal uncertainty is estimated as the standard deviation of the horizontal distribution of conversion points at their corresponding depths. In translating layer thicknesses to discontinuity depth in the following sections, station elevations have been taken into account.

It is reasonable for the waveform fitting (WFF), insensitive to the crustal *P* velocity, to use κ constrained by the HKS. We designed two velocity models at station SS83 for the WFF in the same domain as the HKS to search the Moho thickness and κ: one has a *P* velocity of 6.456 km/s and the other has a *P* velocity of 7.000 km/s. The resultant imaging of the first model (Figure S7) shows that the Moho is located at a depth of 49.5 km and κ is 1.66, which is consistent with 48.2 km derived by the WFF with the constraint of κ (1.69) by the HKS (Figure 4b). For the second model, the Moho is imaged at a depth of 52.7 km and κ is 1.68 (Figure S7), which agree within uncertainties with those in the first model.

Stacking receiver functions and comparing the waveforms or specific values of the stack with those predicted for crustal models with a range of crustal thicknesses and Poisson's ratios [*Van der Meijde et al.*, 2003; *Zhu and Kanamori*, 2000] is meaningful if the collection of individual RFs is generally coherent. Such coherency is lacking for SPREE stations inside the rift's gravity high, making their stacks more challenging to interpret or compare to predictions (Figures 4c and 4e). Even for stations like SS83, which is well outside the gravity high and for which the $P_m s$ phase stacks coherently, the crustal multiples do not stack coherently (Figure 4f). Intralayer multiples are important for the comparative grid search methods of *Van der Meijde et al.* [2003] and *Zhu and Kanamori* [2000] as they reduce the trade-off between Poisson's ratio and layer thickness in explaining the timing of a *P*-to-*S* converted phase. Because of these incoherencies and the corresponding reduced significance of the stacks, these two methods respond to different aspects of the RFs and thus yield different answers for layer thickness beneath some stations and similar answers at other stations, primarily those outside of the gravity high. An advantage of the *H*-κ method is that its application to individual prestack RFs, and subsequent summation, is less sensitive to noise and waveform complexities than applying the waveform fitting method to individual prestack RFs. However, an advantage of the waveform fitting method is that it also works for thin shallow layers, such as sedimentary layers, where the *H*-κ method has no sensitivity.

Here we apply the *H*-κ method to individual prestack RFs to estimate crustal thickness and average κ. We then apply the waveform-fitting method to estimate the same for the sedimentary layer, if present, then estimate thickness of the remaining one- or two-layer crust by fitting the stacked RF, using the κ from the *H*-κ method or a two-layer crustal model based on the upper portion of NA04 [*Van der Lee and Frederiksen*, 2005] and correcting for sediments.

3. Results

Here we present the results of the SPREE receiver function analysis, with the stations separated into four groups: (1) The SC stations in the Superior Province north of Lake Superior and outside the MGA (Figure 2a), (2) The SN stations that form a line that crosses the gravity high at a near-right angle and at a local, along-axis gravity maximum (Figure 2b); this line is also oriented in roughly the same direction as the incoming teleseismic waves from the two dominating seismicity zones in South America and the north-northwest Pacific (Figures 2b and 3a), (3) the SM stations that follow the MGA gravity maximum along its long axis (Figure 2b), and (4) the SS stations that also cross the MGA roughly at a right angle, but in a place that represents a saddle point in the gravity anomaly and that lies between two sharp turns in the gravity high (Figure 2b). This jog in the gravity high coincides roughly with the Belle Plaine Fault, which was hypothesized by *Chase and Gilmer* [1973] to represent a synrift transform fault similar to those at mid-oceanic ridges. If so, little evidence of rift-related structures might be expected beneath the SS line. In contrast, we would expect the SN line to show typical rift structure. The SM line would connect the rift structures between and beyond the two cross lines.

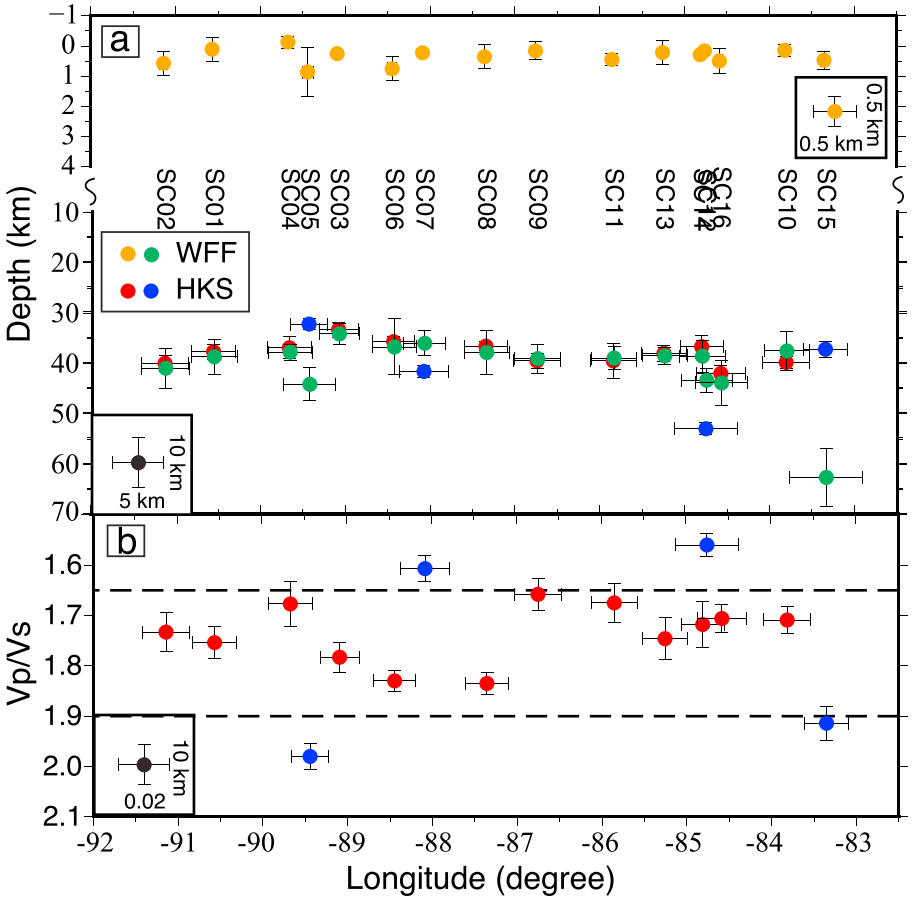

Figure 5. Crustal structure of the Canadian Shield from subgroup SC RFs. a) Crustal layering. A flat, sharp Moho (green/red/blue dots) and a thin sedimentary layer (orange dots) appear. Green and orange dots indicate the results derived by the WFF. Red and blue dots indicate the results derived by the HKS. b) κ (α/β ratio). Red and blue dots indicate stations within and out of a κ range of 1.65-1.90, respectively.

3.1. Subgroup SC, North of Lake Superior

The Moho beneath the SC stations in the Archean Superior Province is sharp and relatively flat (Figure 5). The SC stations show an average Moho depth for this part of the Superior Province of 39.5 ± 5.0 km and an average κ of 1.74 ± 0.11 (Figure 5).

Examination of the record sections of individual RFs for each station reveals that the stations can be clustered into subgroups (Figure S1). One group shows a clear, consistent Moho at a depth of 38.1 ± 2.6 km beneath a western group of stations SC01, 02, 03, 04, and 09, consistent with typical Archean cratons [*Durrheim and Mooney*, 1994; *Lloyd et al.*, 2010; *Laske et al.*, 2013]. From stations with somewhat more complex RFs (SC07 and SC10–SC16), we infer a gradual deepening and increasing complexity of the Moho moving east from Lake Nipigon (Figure 2a). The Moho is also inconsistently recorded in RFs for three stations on the north shore of Lake Superior (SC05, SC06, and SC08), though it appears to be deeper than the Moho in the first group. This inconsistency can be explained through Moho complexity resulting from the MCR, as illustrated for our stations along the western arm of the MCR.

Sedimentary layer thicknesses are small, less than 1 km, and their uncertainties include a zero thickness, which is consistent with this part of the Superior Province being part of the uplifted Canadian shield, which is dominated by Archean basement rocks at the surface beneath a thin veneer of soil and vegetation.

3.2. Across-Rift Profile SN

The crustal structure along profile SN can be separated into three segments: two branches outside the MGA, which border the central segment inside the MGA (stations SN50 to SN58) (Figure 2b). The northwestern branch, composed of stations SN43–SN49, has a Moho interface that gradually deepens southeastward from

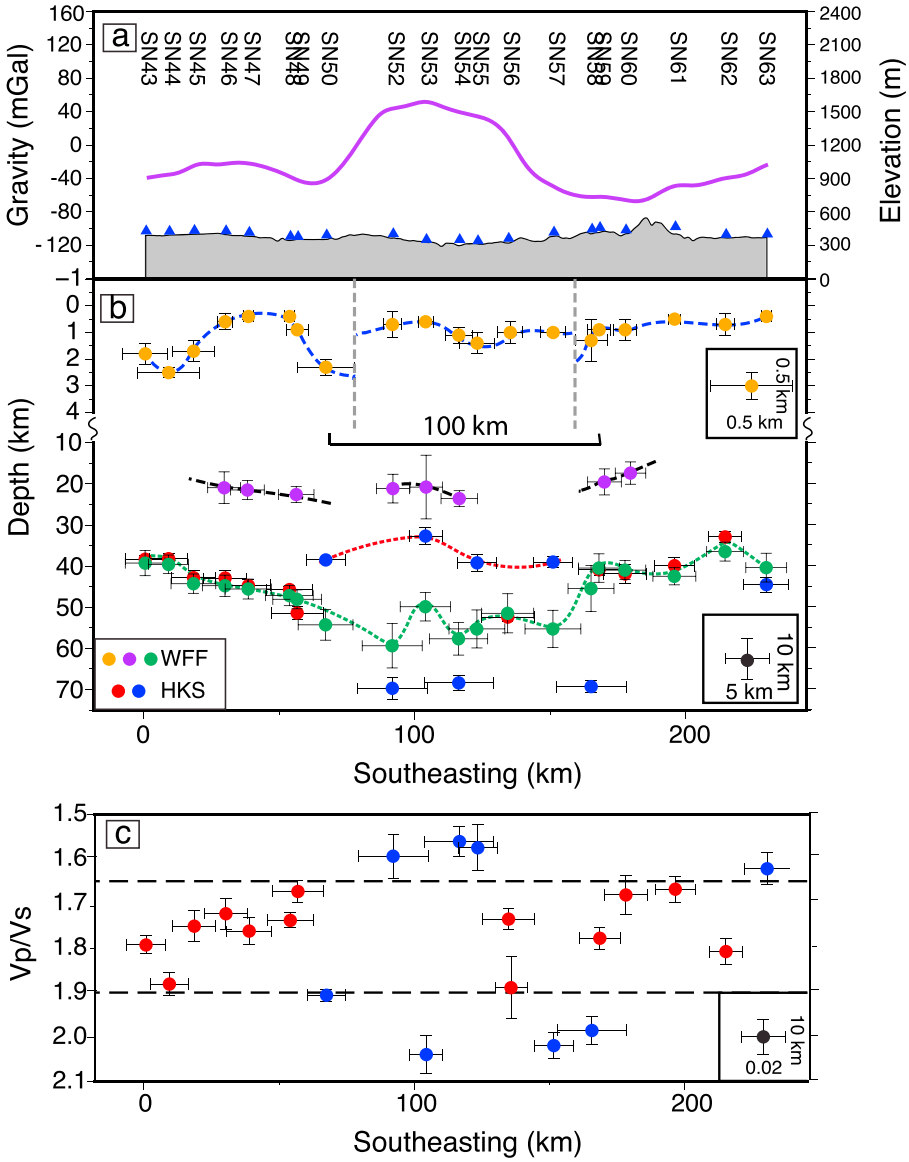

Figure 6. Crustal structure along the across-rift profile SN. (a) Gravity anomaly and surface topography. (b) Crustal discontinuities. Base of sediments is indicated by orange dots, midcrustal discontinuity is represented by purple dots, Moho and bottom of STL are both depicted by green, red, and blue dots, and top of STL is denoted by the red dashed line. WFF and HKS are the modeling methods. A midcrustal discontinuity obtained by the WFF at ~20 km is depicted by purple dots. Green and orange dots indicate the results derived by the WFF. Red and blue dots indicate the results derived by the HKS. In the rift, the STL layer appears between the lower crust and the mantle. (c) κ within and out of a range of 1.65–1.90 are indicated by red and blue dots, respectively.

40 km to 50 km with an average of 44 ± 5 km, while the southeastern branch, comprising stations SN59–SN63, has a relatively flat Moho at an average depth of 41 ± 4 km. Although weakened considerably, the interface associated with the Moho of both branches seem to split into two interfaces; the upper interface continues upward and the lower interface goes downward beneath the central segment (Figure 6). These two central interfaces have average depths of 37 ± 4 km and 55 ± 4 km. This 10–20 km thick transition layer between the overlying crust and underlying mantle is similar in location and shape as the layer of underplated material inferred from the GLIMPCE seismic data beneath Lake Superior [*Tréhu et al.*, 1991]. The values of vertically averaged κ for this layer vary considerably (Figure 6), presumably representing strong compositional variations within the rift's crustal column or limitations in our analysis methods to incorporate the presence of topography and/or layering.

This transitional layer is the cause of the incoherent arrivals in the RFs for station SN55 (Figure 3c) and other stations inside the gravity high. For reasons likely related to the interplay between the waves' incidence angles and interface tilt or relief, the *P* waves from NNW Pacific earthquakes generate the strongest *S* waves at the upper interface while *P* waves from South American earthquakes convert to *S* waves predominantly at the lower interface, the relief of which (Figure 6) causes the *S* waves to scatter significantly (Figure 3c).

To approximate interface depth and impedance contrast, we divided the SN55 RFs into a NW and a SE hemisphere, stacked RFs in each hemisphere, and converted the time axis to approximate discontinuity depth using the velocity model NA04 [*Van der Lee and Frederiksen*, 2005]. NA04 has the crustal simplicity of continentally or globally averaged seismic models but incorporates smooth variations within our study region. The result is shown in Figure 4e, along with a similar conversion for a single stack of all RFs for station SS83 (Figure 4f). Figure 4 clearly shows that the lower interface is ill defined: *P* energy is converted over a broad depth range, which could be the result of strong relief on the interface, coarse or fine lamination, or a gradual change in seismic velocity over a ~10 km depth range. The upper interface, around 35 km depth, presents a sharper, stronger velocity contrast that is similar to the relatively simple, deeper Moho contrast found for station SS83. This similarity suggests that the upper interface could represent the original Moho, which may have been uplifted, likely during a crustal-thinning stage of rifting, by as much as 10 km compared to the surrounding terrain (Figure 6). A straightforward explanation for the material between this uplifted, original Moho and the actual mantle beneath the lower interface would be underplated volcanic material, analogous to that modeled beneath the Lake Superior segment of the MCR [*Tréhu et al.*, 1991]. Additionally, the transitional layer could represent a mixture of crustal, mafic, and underplated materials, rendering the concept of a Moho ambiguous.

In addition to the transitional, possibly underplated material between the crust and mantle beneath the MGA, hints of three segments of a midcrustal discontinuity are observed around a depth of ~20 km (Figure 6b). Given the complex nature of the crust-mantle interface (Figures 3, 4, and 6) and the well-documented faulted and volcanic nature of the shallow crust beneath the MGA [*Miller and Nicholson*, 2013; *Ojakangas et al.*, 2001], it is unlikely that the midcrustal section beneath the MGA remained undisturbed. The thin sedimentary cover above this midcrustal discontinuity makes it unlikely that it is an artifact from reverberations within the sedimentary cover. We hypothesize that this segmented apparent midcrustal discontinuity either represents the bottom of the rift deposits or represents an intermittent Conrad discontinuity. While it is possible for the seismic impedance of the rift deposits to contrast sharply with the underlying crust, it is not required that this impedance contrast sharply occurs over a narrow depth range, especially if the rift deposits contain metasedimentary rocks. In both cases, its segmented appearance would be consistent with the location of rift-flanking faults between the segments. These faults have been documented in various on-land gravity and seismic studies [e.g., *Cannon et al.*, 1989; *Chandler et al.*, 1989; *Hinze et al.*, 2005] and could have accommodated normal faulting during rifting as well as postrift reverse faulting.

The gravity lows that flank the gravity high of the MGA (Figure 6) are typically successfully modeled with the margins of a sedimentary basin that existed during rifting [*Tréhu et al.*, 1991; *Thomas and Teskey*, 1994; *Chandler et al.*, 1989; *Soofi and King*, 1999]. We find the thickest sediments to be 2.5 and 1.5 km thick, respectively, beneath stations SN50 and SN58, which flank the rift. Within each of the three segments of the SN station line, the variations of the sedimentary layer thickness are remarkably consistent with gentle undulations in the gravity anomaly, which was not used to constrain our model. However, the average gravity anomaly for the central segment is much higher than for the outer segments. The main reason for this is that the stack of volcanic material that increases gravity beneath the central segment is thicker and uplifted compared to the outer segments [*Chandler et al.*, 1989].

3.3. Along-Rift Profile SM

The SM line follows the gravity high from the southwestern tip of Lake Superior to the Minnesota-Iowa border. The line has a wide station gap near the center at the cities of Minneapolis and St. Paul, where seismic noise is too high to allow useful observations for this study. The SM line intersects the SN line at station SN53 and the SS line at station SS73 (Figure 2b).

The observed transitional layer between the crust and mantle beneath the central segment along the SN line is present all along the SM line (Figure 7), though it varies in depth, thickness, relief, and sharpness of its interfaces. The average depth of the transitional layer gradually deepens toward the south. On the northern two thirds of the line the upper interface is at 36–44 km depth, and the lower interface is at the 45–54 km

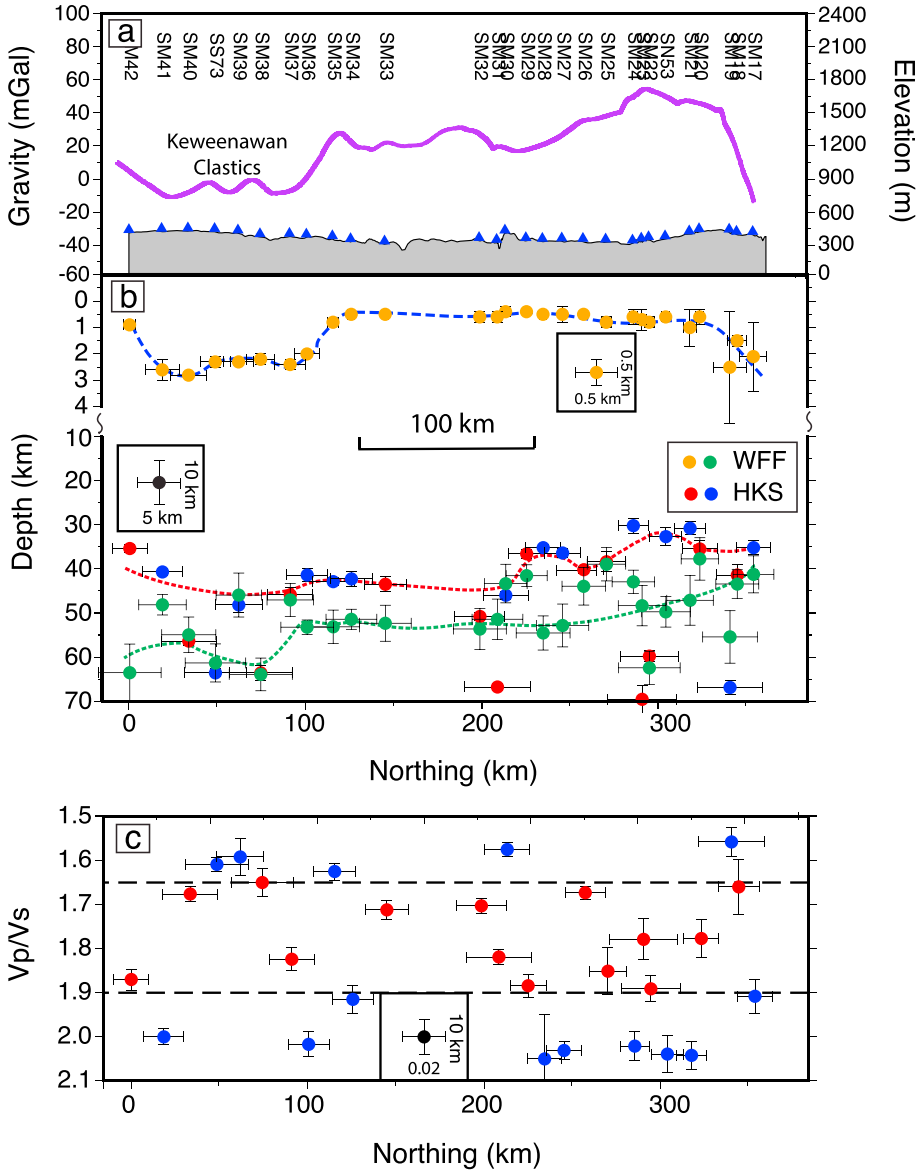

Figure 7. Crustal structure along profile SM. Plotting conventions as for Figure 6.

depth range. Beneath the southern third of the SM line we find the upper interface in the 42-47 km range, while the lower interface is in the 55–60 km depth range. Thus, the subcrustal transition layer (STL) is about 10–14 km thick all along the rift's axis, and this STL is a persistent crustal structure of the MCR.

We also observe the sedimentary layer along the SM line. Sediment thicknesses are bimodal. A roughly 2.5 km thick layer appears along the jog under the southern third of the line, where the gravity high is relatively low (around −10 mGal). On the northern two thirds of the line, the sediment is $\leq$0.5 km thick and the gravity anomaly is higher, from around 20 mGal to >50 mGal. Where the SM line descends from the gravity high upon its far northern side, we also see a corresponding increase in sedimentary thickness and a dramatic thinning in the subcrustal transition layer. On the opposite end, the south side of the SM line, the gravity anomaly increases again, sediments thin, and the subcrustal transition layer remains present. There is no significant correlation between the thickness of the subcrustal transition layer and the strength of the gravity high. If our interpretation of the transition layer as underplated volcanics is correct, its presence beneath the southern third of the SM line along with the associated gravity low and apparent undisturbed sedimentary layer would suggest that the MGA's jog was indeed actively rifting along with the rest of the MCR but was spared from the postrift compression that uplifted the sediments and underlying volcanics, causing a gravity high in the rest of

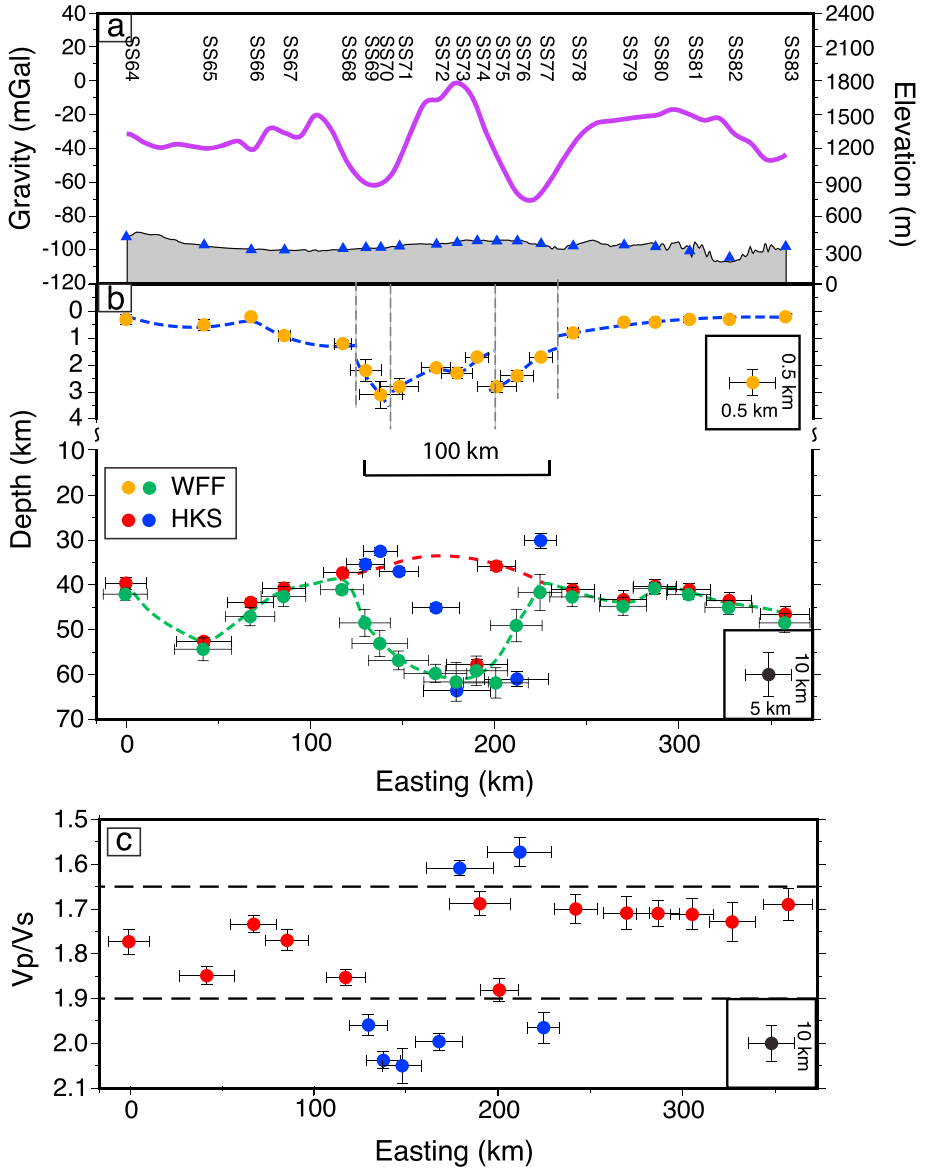

Figure 8. Crustal structure along profile SS. Plotting conventions as for Figure 6. Note that the depression of the Moho is evident.

the MCR. This suggests that the postrift compression may have had a strong directional component that was relatively parallel to the MGA's jog's center segment (near the Belle Plaine Fault) and relatively perpendicular to the northern two thirds of the MGA on the SM line. This directionality would also imply a transpressional component for the MCR's segment that curves beneath Lake Superior, evidence of which has been observed in the GLIMPCE seismic lines [*Cannon et al.*, 1989]. If *Chase and Gilmer* [1973] were right in that this southern Minnesota jog in the MGA represents a rift-related transform fault, it would have had to form after considerable underplating had already taken place. Alternatively, this segment of the MGA is a bona fide part of the MCR that experienced similar rifting to the rest of the MCR but, as mentioned, did not undergo postrift compression. In either case, it is possible and even likely that such a compressional regime would have supported some strike-slip or transpressional motion along the center of the jog or Belle Plaine Fault (Figure 2b).

3.4. Across-Rift Profile SS

The SS line obliquely crosses the gravity high near the Belle Plaine Fault Zone (Figure 2b). The crustal structure beneath the SS line is simpler than along the more northern SN line and also has three segments: the western limb, the eastern limb, and the central segment beneath the relative gravity high. The average Moho depth

beneath the western limb (SS64–SS68) is 43 ± 7 km with an outlier of ~55 km beneath the station SS65, whereas that beneath the eastern branch (SS78–SS83) is 43 ± 3 km. Beneath the 84 km wide central segment (SS69–SS77), the Moho is again elusive, showing evidence for an interface around 35 km deep as well as a steeply diving lower interface with a maximum depth of nearly 60 km. The along-line pattern of κ is similar to that across the SN line, with reasonably normal values of 1.65–1.9 for the outer segments, and considerably varying values for the crust in the central segment (Figure 8c).

Also, variations in the thickness of the sedimentary layer are consistent with the trends in the gravity anomaly, with the gravity anomaly's minima at −60 to −70 mGal coinciding with maximum sediment thickness around 3 km beneath stations SS70 and SS75 (Figure 8b). Apparent offsets in the interface at the bottom of the sedimentary layer near the center of the gravity high may reflect transform faulting along the Belle Plaine Fault Zone (or jog in the MGA).

4. Discussion

Our RF analysis provides evidence for a 10–15 km thick, continuous subcrustal transitional layer (STL) that closely follows the gravity high (Figure 9). We also find evidence for a clear, sharp, relatively flat Moho beneath the Archean and Proterozoic terranes bordering the MCR. The doubling, variability, duration, and general weakness of the *P*-to-*S* converted waves associated with the base of the crust directly beneath the MGA suggests that this STL likely represents material that underplated during rifting around 1.1 Ga (Figures 4 and 9). Using large-aperture reflection and refraction seismic data from the GLIMPCE line A, *Tréhu et al.* [1991] detected a similar lower boundary within the MCR beneath Lake Superior, which asymmetrically starts from ~40 km depth at the edges of the rift, becomes deeper, and finally reaches its maximum at 55–60 km depth beneath the rift axis. Other evidence for such an underplated layer has been proposed in a number of models for the MCR [e.g., *Thomas and Teskey*, 1994]. Beneath station SPMN, which occupies the urban gap in the SM line (Figure 2b), *Shen et al.* [2013] inferred a Moho at a depth of 47.6 ± 5.6 km, which represents the middle of our STL, while the error bar of *Shen et al.* [2013] comprises the thickness of our STL. The corresponding RF for SPMN indeed shows a weaker, broader *P*-to-*S* converted wave than for transportable array stations away from the MGA [*Shen et al.*, 2013].

As demonstrated by the positive polarity of *P*-to-*S* waves converted at both the upper and lower boundaries of the STL (Figure 3d), the density and *P* and *S* velocities of the STL should be in between those of the overlying lower crust and the underlying lithospheric mantle. The lower interface of the STL is on average ~10 km deeper and the upper interface is on average ~4 km shallower than the Moho outside of the MGA. A density model along GLIMPCE profile A by *Tréhu et al.* [1991] and *Shay and Tréhu* [1993] provides average densities of the lower crust, STL, and lithospheric mantle of 2.80 g/cm^3, 3.10 g/cm^3, and 3.25 g/cm^3, respectively.

Given that the upper part of the underplated layer takes up space otherwise occupied by less dense lower crust while the lower part takes up space normally occupied by denser mantle, the combined effect of this underplated layer on the overall gravity anomaly is subtle at best. A simple calculation using the densities of *Tréhu et al.* [1991] shows that a 14 km thick rectangular STL with a top interface 4 km above the surrounding Moho contributes little to the already strong gravity anomalies that are dominated by shallower structures [*Levandowski et al.*, 2015]. However, assuming a more realistic shape and laterally varying depth and thickness of this layer will cause a somewhat larger gravity anomaly that could further constrain the properties, depth, and shape of the underplated layer imaged here only with RFs.

Interestingly, the Belle Plaine Fault region in south Minnesota appears to be equally underplated (Figures 2b, 9b and 9c). The underplated layer, contributing negligibly to the gravity as described above, implies the existence of intracrustal volcanics near the surface to explain the gravity high beneath the central rift of profile SS. Our RF analysis rather points to minimal uplift of the central stack of igneous rocks, which remains buried beneath about 3 km thick sediments. This minimal uplift and observed shear faulting along this fault could be directly related to the different orientation of the rift along the jog. Such orientation differences could have been amplified by differences in relative dominance between rift-parallel and rift-perpendicular components of the compressional forces on originally subtly and differently oriented segments of the rift.

Our RF analysis also provides depth estimates for the base of the sedimentary cover. Variations in this base correlate with trends in gravity anomalies and are particularly consistent with the local and regional gravity lows (Figures 6–8). Despite the presence of sedimentary rocks, the MCR is marked by a high gravity anomaly

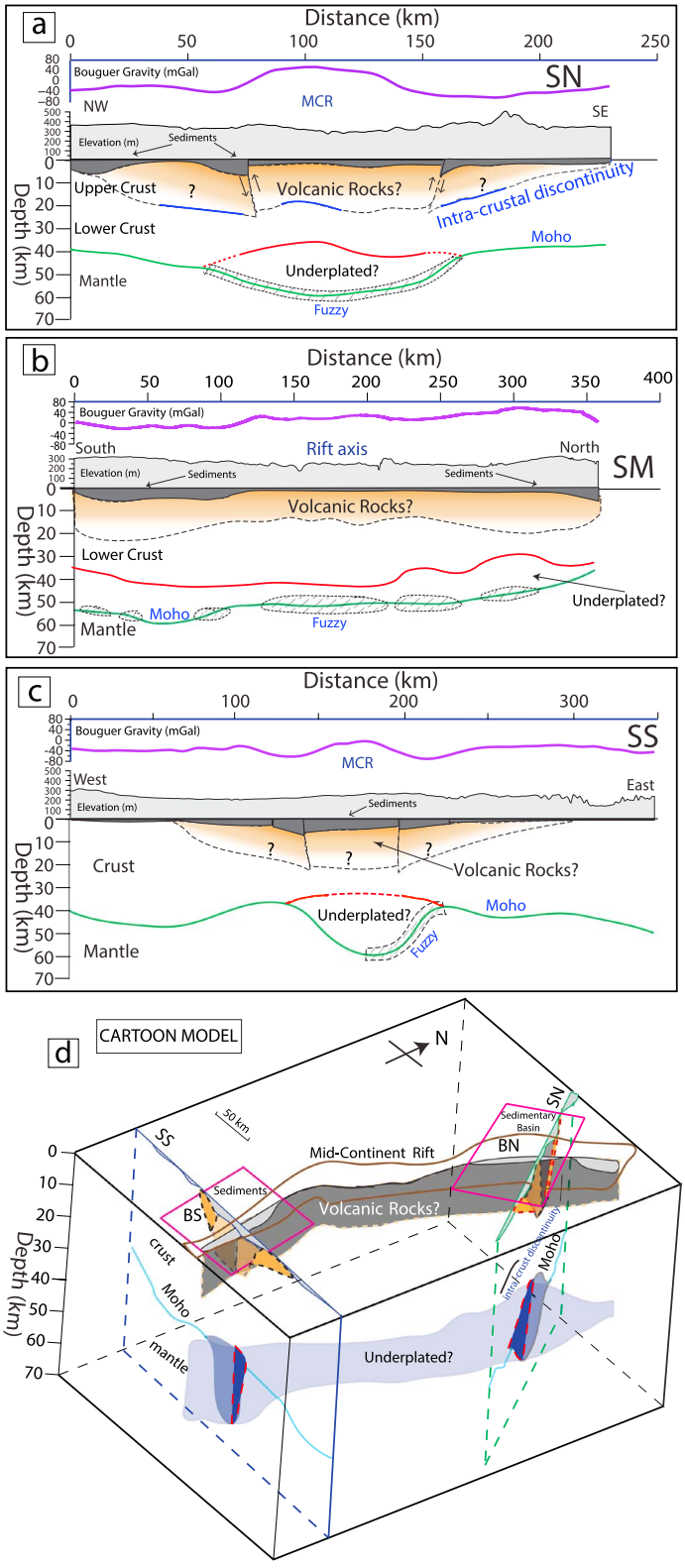

Figure 9. Interpretative models of the crustal structure of the MCR based on profiles (a) SN, (b) SM, and (c) SS. The STL appears along profiles SN and SM, but parts of its bottom boundary of the STL are fuzzy. (d) Three-dimensional cartoon crustal model. Two sedimentary basins are located at and near the interception of profile SM with SN and SS. The low gravity anomaly at the flanks originates from the sediments, whereas the higher gravity anomaly at the rift's long axis reflects the high-density volcanics, shown schematically (orange). The STL is colored violet.

(Figure 9). Since the STL has only a minor effect on the gravity, this requires a shallower high-density crustal layer in the rift. Mafic volcanics from the surface to a depth of 20–35 km have been detected along the GLIMPCE lines [*Tréhu et al.*, 1991; *Shay and Tréhu*, 1993; *Cannon et al.*, 1989; *Hinze et al.*, 1990; *Thomas and Teskey*, 1994]. Gravity modeling along a line in between the SN and SS lines has placed the base of the volcanic layer at ~10 km, with the center of the layer uplifted along inward dipping reversed normal faults [*Chandler et al.*, 1989; *Soofi and King*, 1999]. Because of the continuity of the gravity high, we infer that a thick stack of extruded volcanic rocks underlies the sediments at the center of the MGA and that this stack is offset from its thinner, deeper flanks beneath thicker sediments along reversed normal faults (Figure 9). It is possible but not necessary that the apparent midcrustal discontinuity inferred intermittently for the SN line is related to the base of such a stack of intracrustal volcanic rocks (Figure 6).

Figure 9 shows a synthesis of our analysis of the RFs for all of the SC, SN, SM, and SS lines as a crustal model for a prominent part of the MCR. This model includes a rift basin filled with a thick stack of extruded volcanic rocks and an overlying sedimentary layer, the center of which was uplifted along the MGA during postrift compression. These structures are underlain by Precambrian lower crust and a subcrustal underplated magmatic layer along the MGA (Figure 9).

This crustal structure may be the result of the evolution of the MCR through various stages [*Cannon*, 1992; *Miller and Nicholson*, 2013]. First, mafic magmas, which derive from the mantle, intruded the crust. These volcanic rocks then became more diverse, including more felsic magmas with evidence of "contamination" via crustal melting [*Miller and Nicholson*, 2013]. This stage was followed by crustal subsidence, normal faulting, and crustal thinning, followed by another main period of shallow magmatism that emplaced most of the currently preserved magmatic rocks within the MCR. At some point in the rifting sequence, voluminous mafic magmas would have ponded beneath the crust (underplating) [*Miller and Vervoort*, 1996]. Volcanic rocks at the surface were subsequently, during continuing subsidence, covered with various sediments, for example, the Oronto and Bayfield groups in the Lake Superior region [*Ojakangas et al.*, 2001; *Miller and Nicholson*, 2013; *Stein et al.*, 2014]. The final stage included the compressional stage that reversed the subsidence into uplift in the center of the MGA. NW directionality of the compression during this stage could have led to transpressional faulting in the Lake Superior region and perhaps a small amount of strike-slip faulting in southern Minnesota along the MGA's jog/Belle Plaine (transform) Fault Zone. The presence of a relatively voluminous, deep underplated layer and the relatively undisturbed sediments, which are both inferred from our RF analysis, along with the local gravity saddle point implying a less uplifted intracrustal dense body (e.g., igneous rocks), suggest that this rift segment was a regular rift segment rather than an mid-ocean ridge-like transform fault that would have offset the sedimentary and the underplated layer beneath the center of the fault.

The presence of the underplated layer inferred from our RF analysis is supportive of the hypothesis that a mantle plume started the MCR, but the linear extent of the underplated layer along the entirety of the MCR in our study region is not as easily reconciled with a typical, near-cylindrical mantle plume.

5. Conclusions

P wave receiver functions from 82 SPREE stations reveal remarkably consistent and contrasting crustal structures associated with the most prominent part of the MCR, from Lake Superior to Iowa. In the general study region outside of the MCR, the SPREE RFs are consistent with a reasonably sharp Moho beneath the Precambrian terranes that were cut by the MCR around 1.1 Ga ago. The Moho beneath the Archean Superior Province north of Lake Superior and beneath the western Proterozoic Penokean Province south of Lake Superior (Figure 1) is found at an average depth of around 40 km and appears to be the flattest within our study region. The Moho beneath the Superior Province of the continental platform west of the MCR and its boundary with the Proterozoic Yavapai Terrane east of the MCR is less flat and tends to lie somewhat deeper than 40 km. Our RF analysis confirms that the Superior Province is covered by a sedimentary layer that ranges in thickness from zero to at most a few hundred meters. Though the total thickness of sedimentary layer varies from station to station, the overall thickness increases toward the south and reaches maximum thickness ~3 km in the flanks of the MCR in southeastern Minnesota, where the gravity anomalies are strongly negative. Even along the rift's gravity high, nearly 3 km of sediments are found where the SPREE SS line crosses the rift (Figure 1). At this point, the gravity high is correspondingly minimal, marking a saddle point in the anomalous gravity field.

The Moho beneath the crustal MCR structures is a consistently elusive feature all along the MCR in our study region (Figures 6–8) and likely beyond [*Tréhu et al.*, 1991; *French et al.*, 2009; *Moidaki et al.*, 2013;

Shen et al., 2013]. RFs of stations along the gravity high (the SM line) do not show a similar, clear *P*-to-*S* converted phase peak around 5 s as the other SPREE stations do (Figure 3). Instead, they show *S* wave energy that is systematically weak, bimodal in arrival time, or long in duration. Multiple analyses of these and other RFs lead us to believe that the crust of the MCR is underlain by a 10–15 km thick subcrustal transitional layer with less dense and seismically slower material than the underlying mantle. If the upper interface represents the bottom of the crust, the subrift crust would be slightly thinner than the crust outside the MGA. If one subtracted the layers of intruded and extruded basalts from the subrift crust, the remaining crust would be considerably thinner than the surrounding crust. The upper and lower interfaces of this layer have varying impedance contrasts, dips, and other relief. We have interpreted this layer as representing cooled magmatic material that underplated the crust during rifting following a scenario, for example, as described by *Miller and Nicholson* [2013]. The SN and SS station lines show that this underplated layer is thickest beneath the rift's center, thins toward the rift's flanks, and is absent away from the rift.

For some stations along only the SN station line, our RFs show evidence of a potential intermittent mid-crustal discontinuity. It is possible that this discontinuity marks an interface between the lower crust and the overlying, primary stack of volcanics that extruded during the main stage of rifting [*Miller and Nicholson*, 2013]. Alternatively, this evidence could reflect reverberations within the sedimentary column. The intracrustal presence of thick piles of igneous rocks has been inferred in numerous preceding studies, mostly from the high gravity and magnetic anomalies, and in some places, like Lake Superior, via surface exposures and seismic sounding (GLIMPCE and Norpac [*Cannon et al.*, 1989; *Tréhu et al.*, 1991; *Hinze et al.*, 1997]).

In southeastern Minnesota the gravity high is relatively weak and oriented nearly at right angles to that to the north and south. *Chase and Gilmer* [1973] report that geologic offsets have been documented along the Belle Plaine Fault Zone there and interpreted it as a transform fault like those at mid-oceanic ridges. However, the underplated layer is as thick beneath this segment as beneath the stronger segments of the gravity high, and this rift segment is underlain by very nearly the same amount of sediments as the rift's deepest flanks. A minor gravity high at the center of the MGA suggests that a pile of igneous rocks lies buried beneath the sediments, just as elsewhere along the rift. However, in contrast to elsewhere along the rift, the southeastern Minnesota rift segment experienced much less postrift reverse faulting and associated erosion of the central sediments than the rift elsewhere. Based on the new evidence presented here, we conclude that the southeastern Minnesota segment of the MGA does not represent a transform fault but instead represents a "normal" rift segment. Because this segment was oriented relatively parallel rather than perpendicular to the compressive forces that reversed the normal faults in the rift's flanks elsewhere, this rift segment instead experienced transform or transpressional faulting rather than the uplift, sediment erosion, and elevated gravity that is typical for the more prominent segments of the MGA.

Our final conclusion is that the presence of the underplated layer beneath the crustal MCR structures is consistent with the hypothesis that the MCR was initiated by a mantle plume [*Hinze et al.*, 1997; *Miller and Nicholson*, 2013] but that the linear extent of this layer all along the rift's long axis provides a geometric constraint that is less consistent with the notion of a mantle plume.

Acknowledgments
We are grateful to the Editor Martha Savage and anonymous reviewers for insightful comments, which improve the manuscript dramatically. We thank all the landowners that hosted a SPREE seismic station and service crews on their land during 2.5 years (http://www.earth.northwestern.edu/spree/Welcome.html, and https://twitter.com/seismoSPREEDOM). All the SPREE data are available at IRIS-DMC (http://ds.iris.edu/ds/nodes/dmc/data/) and all the RFs derived in this study are available upon request. This research was funded by NSF grants EAR-0952345 to Van der Lee et al. and EAR-1148088 to Stein et al. We thank Bill Hinze, Will Levandowski, Weisen Shen, and two anonymous reviewers for constructive comments that improved the manuscript.

References

Allen, D., W. Hinze, and W. Cannon (1992), Drainage, topographic, and gravity anomalies in the Lake Superior region: Evidence for a 1100 Ma mantle plume, *Geophys. Res. Lett.*, *19*(21), 2119–2122.

Behrendt, J. C., A. G. Green, W. F. Cannon, D. R. Hutchinson, M. Lee, B. Milkereit, W. F. Agena, and C. Spencer (1988), Crustal structure of the Midcontinent Rift System: results from GLIMPCE deep seismic reflection profiles, *Geology*, *16*, 81–85.

Berteussen, K. (1977), Moho depth determinations based on spectral-ratio analysis of NORSAR long-period P waves, *Phys. Earth Planet. Inter.*, *15*(1), 13–27.

Cannon, W. (1992), The Midcontinent rift in the Lake Superior region with emphasis on its geodynamic evolution, *Tectonophysics*, *213*(1), 41–48.

Cannon, W., et al. (1989), The North American Midcontinent rift beneath Lake Superior from GLIMPCE seismic reflection profiling, *Tectonics*, *8*(2), 305–332.

Chandler, V. W., P. L. McSwiggen, G. B. Morey, W. J. Hinze, and R. R. Anderson (1989), Interpretation of seismic reflection, gravity, and magnetic data across middle Proterozoic mid-continent rift system, northwestern Wisconsin, eastern Minnesota, and central Iowa, *AAPG Bull.*, *73*(3), 261–275.

Chase, C., and T. Gilmer (1973), Precambrian plate tectonics: The midcontinent gravity high, *Earth Planet. Sci. Lett.*, *21*, 70–78.

Chulick, G., and W. Mooney (2002), Seismic structure of the crust and uppermost mantle of North America and adjacent oceanic basins: A synthesis, *Bull. Seismol. Soc. Am.*, *92*(6), 2478–2492.

Durrheim, R. J., and W. D. Mooney (1994), Evolution of the Precambrian lithosphere: Seismological and geochemical constraints, *J. Geophys. Res.*, *99*(B8), 15,359–15,374.

French, S. W., K. M. Fischer, E. M. Syracuse, and M. E. Wysession (2009), Crustal structure beneath the Florida-to-Edmonton broadband seismometer array, *Geophys. Res. Lett.*, *36*, L08309, doi:10.1029/2008GL036331.
Gordon, M., and M. Hempton (1986), Collision-induced rifting: The Grenville Orogeny and the Keweenawan rift of North America, *Tectonophysics*, *127*(1), 1–25.
Green, J. (1982), 5: Geology of Keweenawan an extrusive rocks, *Geol. Soc. Am. Mem.*, *156*, 47–56.
Green, A. G., W. G. Cannon, B. Milkereit, D. R. Hutchinson, A. Davidson, J. C. Behrendt, C. Spencer, M. W. Lee, P. Morel-à-l'uissier, and W. F. Agena (1989), A "GLIMPCE" of the deep crust beneath the Great Lakes, in *Properties and Processes of Earth's Lower Crust*, vol. 51, edited by R. F. Mereu, S. Mueller, and D. M. Fountain, pp. 65–80, AGU, Washington, D. C. Geophys. Monogr. Ser.
Hinze, W. J., D. Allen, L. Braile, and J. Mariano (1997), The Midcontinent rift system: A major Proterozoic continental rift, *Geol. Soc. Am. Spec. Pap.*, *312*, 7–36.
Hinze, W. J., et al. (2005), New standards for reducing gravity data: The North American gravity database, *Geophysics*, *70*(4), J25–J32.
Hinze, W. J., L. Braile, and V. Chandler (1990), A geophysical profile of the southern margin of the Midcontinent Rift System in western Lake Superior, *Tectonics*, *9*(2), 303–310.
Keller, G. R., D. R. Russell, W. J. Hinze, J. E. Reed, and P. C. Geraci (1980), Bouguer gravity anomaly map of the east-central midcontinent of the United States, *U.S. Nucl. Regul. Comm. NUREG 1 CR1663*, U.S. Nucl. Regul. Comm., Springfield, Va.
Kennett, B. (1979), The suppression of surface multiples on seismic records, *Geophys. Prospect.*, *27*(3), 584–600.
King, E., and I. Zietz (1971), Aeromagnetic study of the midcontinent gravity high of central United States, *Geol. Soc. Am. Bull.*, *82*(8), 2187–2208.
Langston, C. (1979), Structure under Mount Rainier, Washington, inferred from teleseismic body waves, *J. Geophys. Res.*, *84*(B9), 4749–4762.
Laske, G., G. Masters, Z. Ma, and M. Pasyanos (2013), Update on CRUST1.0—A 1-degree global model of Earth's crust, Abstract presented at EGU2013-2658 at 2013 EGU General Assembly, Vienna, Austria, 7–12 Apr.
Levandowski, W., O. S. Boyd, R. W. Briggs, and R. D. Gold (2015), A random-walk algorithm for modeling lithospheric density and the role of body forces in the evolution of the Midcontinent Rift, *Geochem. Geophys. Geosyst.*, *16*, 4084–4107, doi:10.1002/2015GC005961.
Ligorría, J., and C. Ammon (1999), Iterative deconvolution and receiver-function estimation, *Bull. Seismol. Soc. Am.*, *89*(5), 1395–1400.
Lloyd, S., S. van der Lee, G. S. Franca, M. Assumpcao, and M. Feng (2010), Moho map of South America from receiver functions and surface waves, *J. Geophys. Res.*, *115*, B11315, doi:10.1029/2009JB006829.
McWilliams, M., and D. Dunlop (1978), Grenville paleomagnetism and tectonics, *Can. J. Earth Sci.*, *15*(5), 687–695.
Miller, J. D., and J. D. Vervoort (1996), The latent magmatic stage of the Midcontinent rift: A period of magmatic underplating and melting of the lower crust, paper presented at 42nd Annual Meeting on Institute on Lake Superior Geology, pp. 33–35, Cable, Wisconsin.
Miller, J. D., and S. W. Nicholson (2013), Geology and mineral deposits of the 1.1 Ga Midcontinent rift in the Lake Superior Region—An overview, in *Field Guide to the Copper-Nickel-Platinum Group Element Deposits of the Lake Superior Region, Duluth, MN*, edited by J. Miller, Precambrian Research Center Guidebook 2013-01 pp. 1–50.
Moidaki, M., S. S. Gao, K. H. Liu, and E. Atekwana (2013), Crustal thickness and Moho sharpness beneath the Midcontinent rift from receiver functions, *Res. Geophys.*, *3*(1), 1–7.
Ojakangas, R. W., G. B. Morey, and J. C. Green (2001), The Mesoproterozoic midcontinent rift system, Lake Superior region, USA, *Sediment. Geol.*, *141*, 421–442.
Shay, J., and A. Tréhu (1993), Crustal structure of the central graben of the Midcontinent Rift beneath Lake Superior, *Tectonophysics*, *225*(4), 301–335.
Shen, W., M. Ritzwoller, and V. Schulte-Pelkum (2013), Crustal and uppermost mantle structure in the central U.S. encompassing the Midcontinent Rift, *J. Geophys. Res. Solid Earth*, *118*, 4325–4344, doi:10.1002/jgrb.50321.
Sims, P. K. (1987), *Precambrian Basement Map of the Northern Mid-Continent USA*, pp. 1–12, U.S. Geol. Surv., Reston, Va.
Soofi, M., and S. King (1999), A modified beam analysis effect of lateral forces on lithospheric flexure and its implication for post-rift evolution of the Midcontinent Rift system, *Tectonophysics*, *306*(2), 149–162.
Stein, C. A., S. Stein, M. Merino, G. R. Keller, L. M. Flesch, and D. M. Jurdy (2014), Was the Midcontinent Rift part of a successful seafloor-spreading episode?, *Geophys. Res. Lett.*, *41*, 1465–1470, doi:10.1002/2013GL059176.
Thiel, E. (1956), Correlation of gravity anomalies with the Keweenawan geology of Wisconsin and Minnesota, *Geol. Soc. Am. Bull.*, *67*(8), 1079–1100.
Thomas, M., and D. Teskey (1994), An interpretation of gravity anomalies over the Midcontinent Rift, Lake Superior, constrained by GLIMPCE seismic and aeromagnetic data, *Can. J. Earth Sci.*, *31*(4), 682–697.
Tréhu, A., et al. (1991), Imaging the Midcontinent Rift beneath Lake Superior using large aperture seismic data, *Geophys. Res. Lett.*, *18*(4), 625–628.
Van der Lee, S., and A. Frederiksen (2005), Surface wave tomography applied to the North American upper mantle, in *Seismic Earth: Array Analysis of Broadband Seismograms*, edited by A. Levander and G. Nolet, pp. 67–80, AGU, Washington, D. C.
Van der Meijde, M., S. Van der Lee, and D. Giardini (2003), Crustal structure beneath broad-band seismic stations in the Mediterranean region, *Geophys. J. Int.*, *152*(3), 729–739.
Van Schmus, W., J. Green, and H. Halls (1982), Geochronology of Keweenawan rocks in the Lake Superior region: A summary, *Geol. Soc. Am. Mem.*, *156*, 165–172.
Vervoort, J., K. Wirth, B. Kennedy, T. Sandland, and K. S. Harpp (2007), The magmatic evolution of the Midcontinent rift: New geochronologic and geochemical evidence from felsic magmatism, *Precambrian Res.*, *157*(1), 235–268.
Vinnik, L. (1977), Detection of waves converted from P to SV in the mantle, *Phys. Earth Planet. Inter.*, *15*(1), 39–45.
Whitmeyer, S. J., and K. E. Karlstrom (2007), Tectonic model for the Proterozoic growth of North America, *Geosphere*, *3*(4), 220–259.
Wolin, E., S. van der Lee, T. A. Bollmann, D. A. Wiens, J. Revenaugh, F. A. Darbyshire, A. W. Frederiksen, S. Stein, and M. E. Wysession (2015), Seasonal and diurnal variations in long-period noise at SPREE stations: The influence of soil characteristics on shallow stations' performance, *Bull. Seismol. Soc. Am.*, *105*(5), 2433–2452.
Zhu, L., and H. Kanamori (2000), Moho depth variation in southern California from teleseismic receiver functions, *J. Geophys. Res.*, *105*(B2), 2969–2980.